Smoothing out sandpiles: rotational bulldozing of granular material

Alban Sauret

Smoothing out sandpiles: rotational bulldozing of granular material

Alban Sauret

October 3, 2012

1 Introduction

1.1 Dense granular flow

Predicting the dynamics of dense granular flow plays an important role in engineering and geophysical flow which involve the transport of granular materials such as for instance cereals, rocks or sand. In the past decade, most of the studies have focused on the flow of granular material on inclined surface due to the obvious applications in rock avalanches, landslides and pyroclastics flows [14, 7] (for a review, see e.g. [6]). However, the bulldozing of granular materials, i.e. the action to push the granular material with a blade on a flat plane, has not received so much attention. Indeed, it is not straightforward to build an experimental setup which allows the study of the steady dynamics of bulldozing granular material in a reproducible way. Moreover, the theoretical description of such flow remains complicated as the rheology of dense granular flow is difficult to capture and until quite recently there was no acceptable continuum model for a granular material [9].

In this project, we explore a problem of granular flow on a plane layer: the rotating bulldozing of a sandpile. Starting from an initial sandpile, we use a rotating blade to transport this sandpile and characterize the motion of the granular materials and the shape of the dune built against the blade. The use of a rotating blade instead of a straight blade with a rectilinear motion allows the system to be recirculated and thereby observing the dynamics over long times. In addition, the variation of speed along the blade potentially allows for richer dynamics. Therefore, the aim of this work is to provide the first experimental results with a rotating bulldozer and characterize the key features of the dynamics.

1.2 Bulldozer-related problems

Surprisingly, there are relatively few previous experimental modeling studies of problems of bulldozing sands. The earliest study by Bagnold [2] considers a 2D situation of a plate immersed in a layer of sand of given thickness. Then the plate is pulled at a given force and the amount of material in the dune keeps increasing at the same rate (see figure 1.a). During the build-up of the dune, the velocity of the blade pulled at a given force exhibits some oscillations due to the episodic avalanching of the dune. From laboratory experiments Bagnold, [2] provided a qualitative picture of the shape and the flow in the dune during the build-up (figure 1.b). However, none of these experiments consider the steady regime where

the amount of granular material in the dune does not change. In addition, no quantitative measurement of the shape of the dune or the velocity of the sand has been provided. More recently, some studies focused on the "song of dunes" problem [5, 1]. A possible experimental setup to measure the loud sound emitted by the motion of an avalanche is based on a rotating blade pushing a layer of sand. Here, the dynamics is also non-steady and the quantitative shape of the dune built by the motion of the blade has not been characterized. Another relevant situation which has been studied over the past few years is a wheel or an inclined plow blade with a given angle of attack. The wheel or the blade is free to move vertically in response to the granular material and after few passages on the granular bed a pattern develops on the road which are called washboard ripples [15, 13]. Note that this situation is not used to push or drag granular materials contrary to the bulldozer problem and therefore the dynamics of the sand remains different.

However, none of these studies provide quantitative experimental results of the shape of the dune carried by a bulldozer and especially in a rotating bulldozer where the rotation is susceptible to bring an interesting new dynamics because of the difference of normal velocity along the blade. Here, in addition to our experiments and the quantitative description of the shape of the dune, we will consider the "$\mu(I)$" rheology to describe the dense granular flow as an incompressible liquid with no variation of volume fraction during the dense flow [9]. Such a rheology has been used with success to describe the flow of granular layers on inclined surfaces [6]. In this paper, we will also use a shallow water model as it may allow us to describe the dynamics observed.

1.3 Constitutive law for dense granular flow: the $\mu(I)$-rheology

The description of dense granular flow through the conservation of momentum and mass requires a continuum description of the material. When granular material flows like a liquid, the local tangential stress τ and the local normal stress p are found to satisfy

$$\tau = \mu(I)\, p \quad \text{with} \quad I = \frac{\dot{\gamma}\, d}{\sqrt{p/\rho}} \tag{1}$$

where $\mu(I)$ is an analogue to a coefficient of friction, while ρ and d are the particle density and diameter. Note that I is the inertial number and represents the ratio of an inertial time scale $\sqrt{d^2\, p/\rho}$ and the shear deformation time scale $\dot{\gamma}^{-1}$ [4, 12]. A constitutive relation, the so-called $\mu(I)$-rheology, has been suggested based on experimental and numerical results (see e.g. GdR Midi [12]):

$$\mu(I) = \mu_1 + \frac{(\mu_2 - \mu_1)\, I}{I + I_0}. \tag{2}$$

This coefficient interpolates a friction coefficient between μ_1 at $I = 0$ and $\mu \to \mu_2$ for $I \to \infty$. I_0, μ_1 and μ_2 depend on the material considered (see table 1). Jop et al. have provided a 3D generalization of this constitutive law and successfully compared it to experiments on granular flows on a pile between rough sidewalls [8, 9]. The granular material is still consider as an incompresible fluid with an internal stress tensor σ_{ij} given by:

$$\sigma_{ij} = -p\, \delta_{ij} + \tau_{ij}. \tag{3}$$

	Glass beads	Sand
μ_1	0.38	0.51
μ_2	0.64	0.93
I_0	0.279	0.8

Table 1: Typical values from the literature for the coefficients to use in the $\mu(I)$-rheology [9].

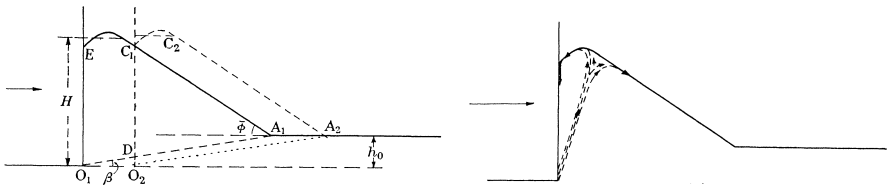

(a) (b)

Figure 1: Schematic of a bulldozed sand heap: (a) shear over a basal shear plane; (b) internal flow (from [2]).

τ is the shear stress which satisfies:

$$\tau_{ij} = \eta(|\dot{\gamma}|, p)\, \dot{\gamma}_{ij} \tag{4}$$

where $\dot{\gamma}_{ij}$ is the strain rate tensor given by $\dot{\gamma}_{ij} = \partial u_i/\partial x_j + \partial u_j/\partial x_i$ and $|\dot{\gamma}| = \sqrt{\dot{\gamma}_{ij}\, \dot{\gamma}_{ij}/2}$ is the second invariant of $\dot{\gamma}_{ij}$. Here p is an isotropic pressure and $\eta(|\dot{\gamma}|, p)$ is an effective viscosity. $\mu(I)$ is given by the relation (2).

The $\mu(I)$-rheology is purely phenomenological but has shown very good agreement with experiments and numerical simulations in different configurations. This model has been implemented in numerical simulations and a good prediction of transient situations such as the granular column collapse has been found [10, 11]. Thoughout this report, we will thus use the $\mu(I)$-rheology in the analytical study.

The remainder of this report is organized as follows: in section 2 we describe the experimental apparatus and in section 3 the phenomenology of the problem. Experiments in a rotating bulldozer exhibits a dynamics which can be separated into two effects: a build-up of the dune perpendicular to the blade over short time-scales and a non-symmetric lateral spreading of the dune over longer time scales. Thus, in section 4 we present the experimental results for the shape of the dune at a given radial position and a simple model is proposed to account for the observed profile. Section 5 is devoted to the lateral spreading of the dune. The final section 6 contains a general discussion and conclusions.

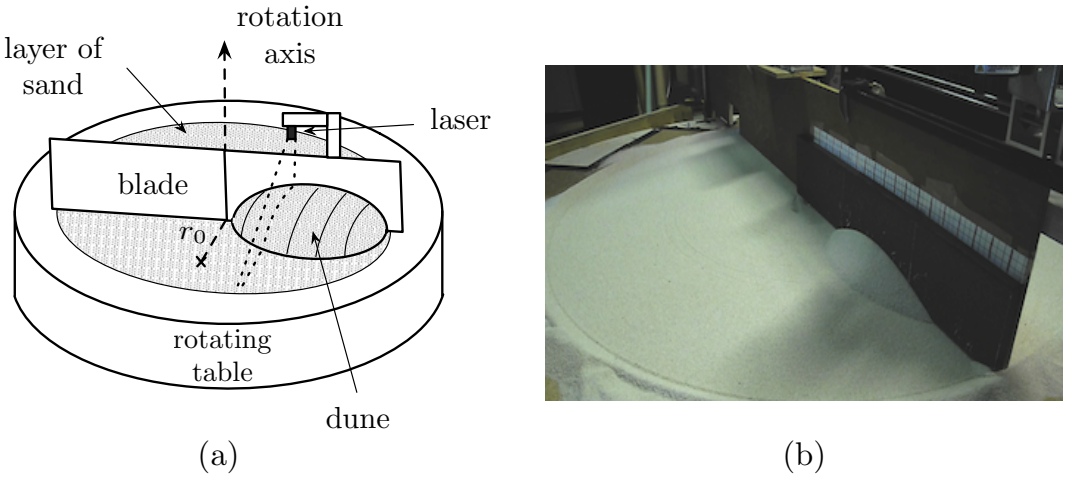

Figure 2: (a) Schematic illustration and (b) photo and of the experimental setup.

2 Experimental setup

2.1 The rotating bulldozer

The experimental apparatus, shown in Fig. 2, consists of a rotating table of 2.2 m diameter which rotates around its axis at an angular velocity Ω. The rotation rate of the table lies in the range 0.05 to 2 rad.s^{-1}.

The surface of the rotating table is coated with sandpaper to suppress slipping of particles on the surface of the table. In the absence of sandpaper, the particles slip on the surface of the table and the structure of the flow is different: the avalanching dune becoming buffered from the upstream static layer by a compressing, sliding layer of grain (see appendix A). In this report, we only focus on the no-slip boundary conditions.

A blade consisting of a flat vertical board, and fixed in the laboratory frame, is secured above the rotating table and acts as a rotating bulldozer (see figure 2(a) & 2(b)). The blade consists of a 1.50 m long and 40 cm height wood plate to which we attach a plywood plate coated with sandpaper to ensure no-slip boundary conditions on the blade. The blade is perpendicular to the surface of the rotating table and is held at a given height around 1 cm. It leads to the presence of an underlying layer of granular materials with a constant thickness. Prior to any experiments, we add granular material on the table which is set in rotation. The granular material build up a bed atop the table. It fills up the gap and its surface is smoothed out by the blade. After a sufficiently long time, we obtain a layer of constant thickness with compaction which does not vary appreciably between two successive experiments. Then, a sandpile is formed by slowly pouring grains onto a selected point on the surface of the existing uniform bed, producing a nearly conical mound with a slope given by the static angle measured previously. We define the initial position of the sandpile as the coordinate of its center, i.e. the radius r_0 from the center of the table where the height of the sandpile is maximum (see figure 2(a)). In the present study, we have used $r_0 = 15$, 25 or 35 cm. Typical parameters used in this study are summarized in table 2.

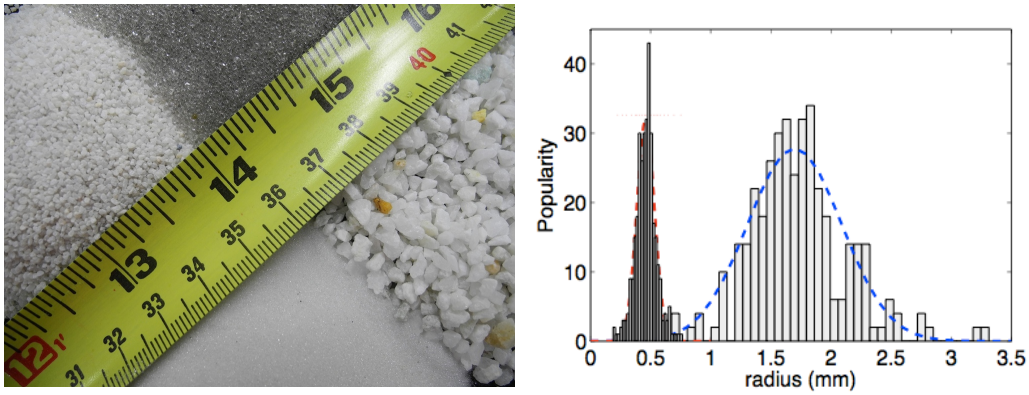

(a) (b)

Figure 3: (a) Photograph of the four granular materials. From left clockwise; aquarium sand ($d = 0.9$ mm), fine glass beads ($d = 0.1$ mm), coarse grit ($d = 3$ mm) and spherical glass beads ($d = 1$ mm). Only results for aquarium sand and spherical glass beads are presented in this report. (b) Size distribution of the coarse grit (white) and the aquarium sand (grey).

Note that in the present bulldozer experiment, because the blade is held at a constant height, no washboard instability is observed [3, 13, 15].

Rotation rate	$0.05 - 2$ rad.s^{-1}
Radius of the blade	0.7 m
Diameter of the particles	0.1 mm - 3 mm
Mass of the dune	0.1 – 1 kg
Initial position of the dune (radially from the center of the table)	15, 25 & 35 cm

Table 2: Range of parameters used in the experiments.

2.2 Granular materials

In this report we present results of bulldozer experiments for different granular media as shown in figure 3(a):
(i) Aquarium sand, of irregular shape, but overall mean diameter of approximately 0.9 mm.
(ii) Spherical fine glass beads (ballotini) of mean diameter 0.1 mm.
(ii) Spherical glass beads (ballotini) of mean diameter 1 mm.
(iv) Coarse grit, of irregular shape, but overall mean diameter of approximately 3 mm.
The size of the aquarium sand and coarse grit particles have been estimated by direct visualization and postprocessing of the picture. Their resulting size distribution is given in figure 3(b). Assuming that the distribution of the particle size can be fitted by a gaussian

distribution, we obtain a distribution of the equivalent radius $r = \sqrt{A/\pi}$ given by

$$N = N_0 \exp\left[-\frac{(r - r_{moy})^2}{2\,\sigma^2}\right]. \tag{5}$$

For example, for the aquarium sand the mean radius of the particle is $r_{moy} \simeq 0.46$ mm and the mean deviation around $\sigma \simeq 0.075$ cm (figure 3(b)). The size distribution of the glass beads were directly obtained from the manufacturer: the size of the fine glass beads[1] ranges in $d = 0.09 - 0.15$ mm and the other glass beads[2] (ballotini) have a size $d = 0.8 - 1.2$ mm.

Then, we can characterize, for the two granular media used in this report, the angle of repose, θ_r, which measures how layers of the medium slide over one another. To estimate a static angle of friction, we make a sandpile of a granular material and measure the typical slope. Rough estimates give an angle of $\theta_r = 22 \pm 2^\circ$ for the 1 mm glass beads and $\theta_r = 44 \pm 4^\circ$ for the aquarium sand . Note that all the experiments were performed in an air-conditioned laboratory maintained at 21°C with humidity controlled. The granular materials were kept dry as moistening the materials, even by a small amount, may have lead to different results.

3 Initial conditions and phenomenology

The initial sandpile is set on the table as described in section 2.1. For each granular material, different initial mass in the sandpile had been considered which leads to different radius and height of the initial sandpile. In addition, the slope of the sandpile is given by a static angle of friction estimated previoulsy. Thus, knowing r_0 the initial radial position of the center of the sandpile and m the mass of granular material in the sandpile allow us to define entirely the system.

The table is then set in rotation, accelerating to a prescribed rotation rate, Ω, or rotation period, T_{rot}, in typically less than 2 seconds (well before the sandpile hits the blade). Thus, the collision of the sandpile and the subsequent dynamics take place at constant rotation velocity. The collision forces a rearrangement of the sandpile into an avalanching dune that is pushed forwards by the blade (figure 4.b). The rearrangement typically takes place in two phases. First, there is a relatively rapid phase (spanning times of order $0.1\,T_{rot}$) in which the dune builds up perpendicular to the blade and adjusts into a quasi-steady shape in that direction (figure 4.c). Thereafter, a slower phase ensues (lasting times of order T_{rot}) in which the dune spreads laterally and shifts radially outwards (figure 4.d).

In the following, we define our system using the coordinate system (x, y, z) (see figure 5.a). The plane (xz) is the plane perpendicular to the blade (see figures 5.a and b). The plane (yz) denotes the plane defined by the blade (see figures 5.a and c). When the table is set in rotation, the center of the sandpile r_0 will hit the blade at the coordinate $r_0 = y_0$. Thus in the following we only refer to y_0 which is the location along the blade where the center of the sandpile hits the blade. In all experiments presented in this report, the height measurement of the dune were done at a distance y which corresponds to the location where the maximum of the dune hits the blade, i.e. $y = y_0$. Experimental observations show that

[1] #8 from Kramer Industries
[2] A-100 from Potters Industries

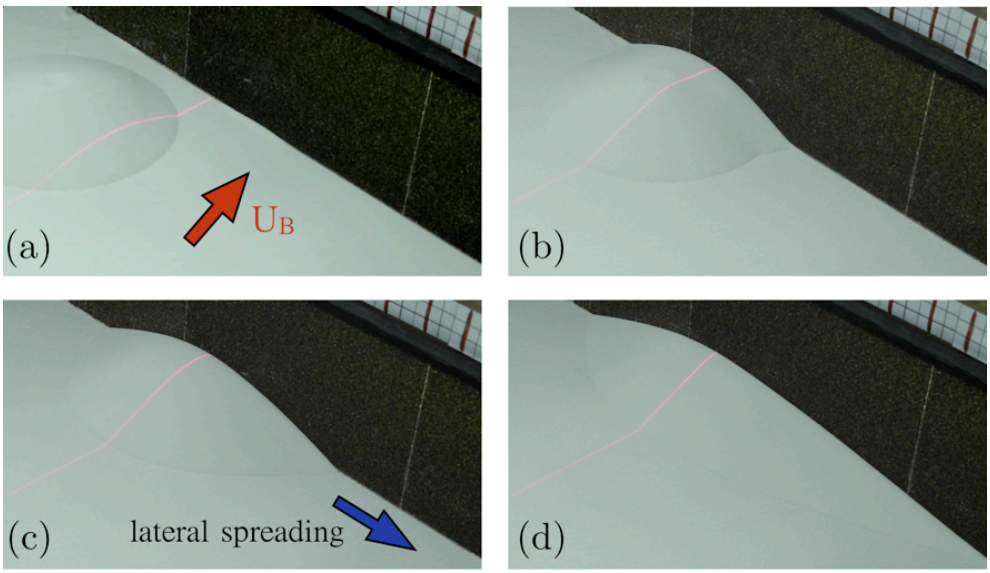

Figure 4: Four successive pictures of the bulldozing sandpile (a) Initial sandpile showing the direction of the underlying layer (red arrow) while the blade is fixed in the laboratory frame. (b) Collision of the sandpile against the blade and quick organization of the dune. (c) Build-up of a quasi-steady structure at a given radius in a short timescale and lateral spreading of the dune (direction indicated by the blue arrow). (d) The slope of the dune at a given radius remains similar but the dune is still subject to lateral spreading. In all pictures, the red laser line is at a constant radius and shows the topography of the dune at this radius.

the time scale $T_x \sim 0.1T_{rot}$ to build-up the dune perpendicularly to the blade, i.e. in the plane (xz), is shorter than the typical time scale $T_y \sim T_{rot}$ for the lateral spreading of the dune in the (yz) plane. Therefore, we split our discussion of the dynamics into two parts. In the next section, we will consider the build-up of a dune perpendicular to the plane and study the typical profile of the dune in the quasi-steady regime that results. Then, we will consider the lateral spreading of the dune using an approximate model for the slope of the dune.

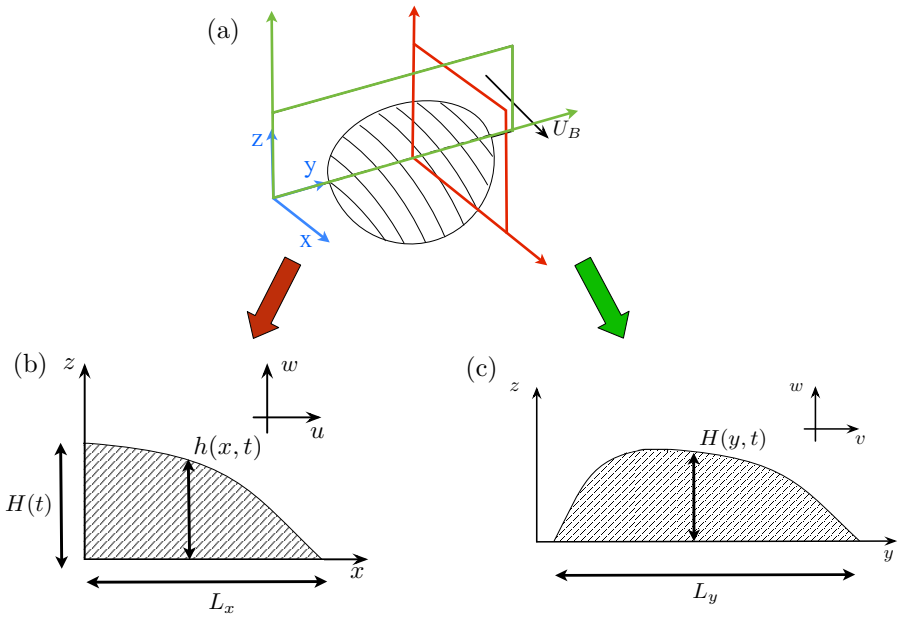

Figure 5: (a) Schematic of the bulldozed dune with the system of coordinates (x, y, z). (b) 2D perpendicular slice in the (xz) plane at a given y-value defining the height $h(x, y, t)$, which reaches a maximum $H(y, t)$ near the bulldozer blade. (c) Front view of the dune in the plane (yz), showing a typical profile of the dune height on the bulldozer blade $H(y, t)$.

4 Dynamics of the dune perpendiculary to the blade

In this section, we consider the profile of the dune in a (xz) plane perpendicular to the bulldozer blade. The non-intrusive method to measure the profile of the dune as a function of the distance to the blade is described in appendix B.

4.1 Experimental observations

Prior to any systematic study, we verify that our experiments are fairly reproducible. Using the aquarium sand, we run two experiments with the same initial conditions, $y_0 = 25$, $m = 1$ kg and the same rotation rate $\Omega = 0.05$ rad/s. Then, we measure the profile of the dune every 5 seconds at a given radial position. The results for two different experiments are illustrated in figure 6 and confirm that the shape of the dune at a given time is fairly reproducible even if the agreement is not perfect. There are two main sources of

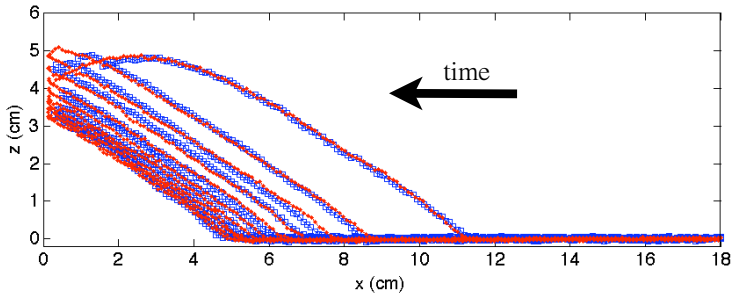

Figure 6: Profile of the dune in a (xz) plane perpendicular to the blade at $y = 25$ cm for $y_0 = 25$, $m = 1$ kg, $\Omega = 0.05$ rad/s. The profiles are taken every 5 seconds (and the direction of time is given by the arrow). The red line and the blue square are two different experiments.

disagreement: the measurement method presented in appendix B has uncertainties around ± 2 mm which already leads to a slight mismatch. In addition to this uncertainties, other disagreement arise because of direct experimental error. For example, the mass of particles to build an initial sandpile is fixed, but the way the particles are packed into the sandpile can be different. Furthermore, the exact position of the initial sandpile can also slightly vary by a few millimeters. Nervertheless, the comparison of two experiments shows that the errors measuring the profile at a given time is much smaller than the profile itself. For a dune against the blade of typical size between 5 and 10 cm, an estimate of the uncertainties would be of the order of a few millimeters. However, we have to notice that the measurement of the profile of the dune for the first few millimeters against the blade is difficult to achieve and therefore the description of the shape of the dune is better along the slope and in the junction with the underlying layer.

Experiments varying the initial mass of aquarium sand in the sandpile for a given initial position $y_0 = 25$ and rotation rate $\Omega = 0.05$ rad/s are shown in figures 7(a), (b), (c) & (d). The size of the initial sandpile depends on the amount of granular material. After a

sufficiently long time to obtain a quasi-steady regime, the dune has a shape similar to a triangle. The size of the dunes are different between all these experiments but their shape seem to remain the same for all mass. It is confirmed by a rescaling of the profile: for all experiments (figure 7(a), (b), (c) & (d)) we rescale the distance by the maximum height $H(y,t)$ (for given y) of the dune at the time considered (which height naturally changes with time). It leads to a nice collapse on a single curve at long time (see figure 7(e)). Therefore, the shape of the dune in the (xz) plane, for low rotation rates seems to be independent of the size of the dune at the scale of our experimental setup.

Note that the results presented in figure 6 and 7 are typical of all the granular material considered in this study. In addition, the gap thicknesses or the low rotation rate does not have a noticeable influence on this shape.

From the rescaled profile, one can consider that the slope will be well fitted by a straight line with an angle equals to the dynamic angle. However figure 7(f) shows that although the shape looks like a dune with a straight slope, there is a slight deviation at the tip (i.e. the furthest distance from the bulldozer blade) of the dune.

4.2 Simple model

4.2.1 Mathematical formulation

We consider granular flow in a slice perpendicular to the bulldozer blade at a given radial position y (see figure 5(b)). Because the time-scale of the motion in the x and in the y directions are different, we assume that in a quasi-steady regime the flow remains two-dimensional in the x direction. We denote $(u(x,z,t), w(x,z,t))$ as the velocity field, $p(x,z,t)$ is the isotropic pressure and τ is the deviatoric stress tensor. The fluid is assumed to be incompressible. The conservation of mass and momentum leads to the governing equations in cartesian coordinates:

$$u_x + w_z = 0, \tag{6}$$

$$\rho\,(u_t + u\,u_x + w\,u_z) = -p_x + \partial_x\,\tau_{xx} + \partial_z\,\tau_{xz}, \tag{7}$$

$$\rho\,(w_t + u\,w_x + w\,w_z) = -p_z - \rho\,g + \partial_x\,\tau_{xz} + \partial_z\,\tau_{zz}. \tag{8}$$

We use the $\mu(I)$ rheology [9] as a constitutive law for the granular material. For the present 2D situation it writes:

$$\tau = p\,\mu(I)\,\frac{\dot\gamma}{|\dot\gamma|}, \qquad \dot\gamma = \begin{pmatrix} 2\,u_x & u_z + w_x \\ u_z + w_x & 2w_z \end{pmatrix}, \quad |\dot\gamma| = \sqrt{4{u_x}^2 + (u_z + w_x)^2}, \tag{9}$$

with

$$\mu(I) = \mu_1 + \frac{(\mu_2 - \mu_1)\,I}{I + I_0}, \qquad I = \frac{|\dot\gamma|\,d}{\sqrt{p/\rho}} \tag{10}$$

In addition, the granular material has to satisfy a no-slip condition on the bottom, at $z = 0$:

$$u(x,0,t) = w(x,0,t) = 0, \tag{11}$$

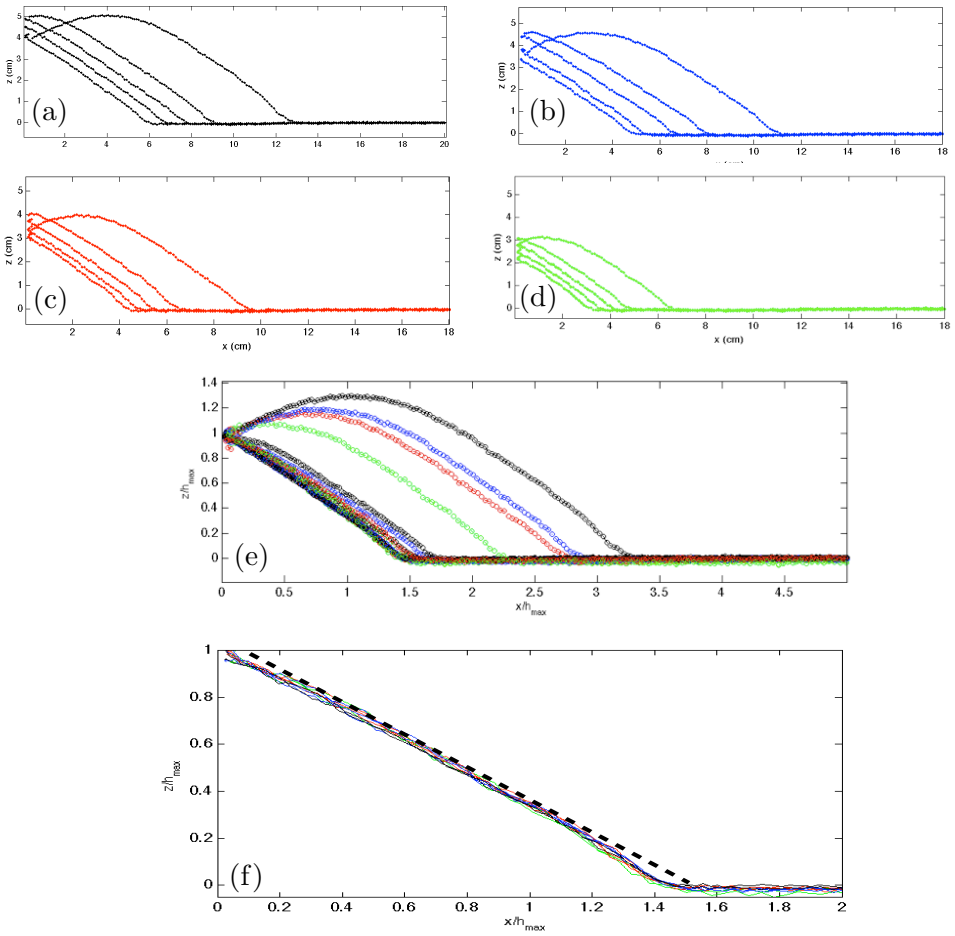

Figure 7: Topography of the bulldozed dune at the radial position $y = 25$ cm for $\Omega = 0.05$ rad/s, $y_0 = 25$ cm and (a) $m = 1000$ g; (b) $m = 750$ g; (c) $m = 500$ g; (d) $m = 250$ g; (e) Rescaled topography of the dune for all the mass considered in (a), (b), (c) and (d). (f) Close-up view of the shape of the dune; the black dotted-line is a straight line. Time go from the right to the left and are taken every 10 seconds.

and is stress-free at its surface, $z = h(x,t)$, leading to:

$$\frac{1}{\sqrt{1+{h_x}^2}} \begin{pmatrix} \tau_{xx} - p & \tau_{xz} \\ \tau_{xz} & \tau_{zz} - p \end{pmatrix} \begin{pmatrix} -h_x \\ 1 \end{pmatrix} = \begin{pmatrix} 0 \\ 0 \end{pmatrix}. \tag{12}$$

Note that the continuity equation (16) can be averaged over the depth of the dune to obtain

$$h_t + \frac{\partial}{\partial x}\left(\int_0^h u \mathrm{d}z\right) = 0. \tag{13}$$

4.2.2 Dimensionless equations

Considering the different variables of the problem, we can make the equations dimensionless by introducing the new variables:

$$x = L\,\hat{x}, \quad z = H\,\hat{z}, \qquad h = H\,\hat{h}, \quad u = U\,\hat{u}, \quad w = \frac{H}{L}\,U\hat{w}, \quad t = \frac{L}{U}\,\hat{t}, \tag{14}$$

$$p = \rho\,g\,H\,\hat{p}, \quad \tau_{ij} = \rho\,g\,\frac{H^2}{L}\,\hat{\tau_{ij}} \tag{15}$$

where L and H denote the characteristic fluid extension and depths respectively (see figure 5(b)). U is a velocity scale, typically the speed of the bulldozer. Then, dropping the hat, the previous equations (6)-(8) can be rewritten as

$$\begin{aligned} u_x + w_z &= 0, & (16)\\ \epsilon\,F^2\,(u_t + u\,u_x + w\,u_z) &= -\epsilon\,p_x + \epsilon^2\,\partial_x\,\tau_{xx} + \epsilon\,\partial_z\,\tau_{xz}, & (17)\\ \epsilon^2\,F^2\,(w_t + u\,w_x + w\,w_z) &= -p_z - 1 + \epsilon^2\,\partial_x\,\tau_{xz} + \epsilon\,\partial_z\,\tau_{zz}, & (18) \end{aligned}$$

where $\epsilon = H/L$ is the aspect ratio of the dune and $F = U/\sqrt{g\,H}$ is the Froude number. The constitutive model of the granular material is given by

$$\tau = p\,\mu(I)\,\frac{\dot{\gamma}}{|\dot{\gamma}|}, \qquad \dot{\gamma} = \begin{pmatrix} 2\,\epsilon\,u_x & u_z + \epsilon^2\,w_x \\ u_z + \epsilon^2\,w_x & 2\,\epsilon\,w_z \end{pmatrix}, \quad |\dot{\gamma}| = \sqrt{4\,\epsilon^2\,{u_x}^2 + (u_z + \epsilon^2\,w_x)^2} \tag{19}$$

with

$$\mu(I) = \mu_1 + \frac{(\mu_2 - \mu_1)}{1 + \mathcal{I}}, \qquad \mathcal{I} = \frac{|\dot{\gamma}|}{\sqrt{p}}\,\mathcal{U}, \qquad \mathcal{U} = \frac{U\,d}{I_0\,H\,\sqrt{g\,H}}. \tag{20}$$

Note also that μ_1 and μ_2 which are directly related to the slope of the dune are also of order ϵ:

$$\hat{\mu_j} = \frac{\mu_j}{\epsilon} \quad j = 1, 2. \tag{21}$$

The boundary conditions now writes:

$$u(x, 0, t) = w(x, 0, t) = 0 \tag{22}$$

and

$$(1 + \epsilon^2\,{h_x}^2)\,\tau_{xz} - 2\,\epsilon\,h_x\,\tau_{xx} = (1 + \epsilon^2\,{h_x}^2)\,p - (1 - \epsilon^2\,{h_x}^2)\,\epsilon\,\tau_{zz}, \tag{23}$$

4.2.3 Long-wave model

To be able to obtain a simple qualitative shape of the dune, we need to introduce a shallow-slope approximation. In this approximation, the ratio of the vertical and horizontal scale of the dune is $\epsilon = H/L \ll 1$. This assumption is quite strong regarding the experimental shape of the dune where $\epsilon \sim 0.2 - 0.5$, however it constitutes a simple way to provide a qualitative shape from analytical studies.

4.3 Quasi-steady case without inertia

In the experiments shown in figure 7, the Froude number is typically of order $F \sim 0.02$. Thus, a first step is to assume that the deviation from a straight slope can be understood assuming that $F \ll 1$ in the equations (17) and (18). Physically, it means that we neglect the inertia of the granular material. This assumption leads to the governing equations:

$$\begin{aligned} u_x + w_z &= 0, & (24)\\ -\epsilon\, p_x + \epsilon^2\, \partial_x\, \tau_{xx} + \epsilon\, \partial_z\, \tau_{xz} &= 0, & (25)\\ -p_z - 1 + \epsilon^2\, \partial_x\, \tau_{xz} + \epsilon\, \partial_z\, \tau_{zz} &= 0. & (26) \end{aligned}$$

Equations (25-26) at the leading-order give:

$$\begin{aligned} p &= (h - z), & (27)\\ \tau_{xz} &= -h_x\,(h - z). & (28) \end{aligned}$$

Then, from the constitutive equation given by the $\mu(I)$-rheology (20), we can write

$$\tau_{xz} = p\mu(I)\,\frac{u_z}{|u_z|} \tag{29}$$

which leads to

$$h_x = -\mu(I). \tag{30}$$

Then, using the constitutive relation given by (20), we obtain

$$h_x = -\mu_1 - \frac{(\mu_2 - \mu_1)}{1 + \mathcal{I}} \qquad \text{with} \qquad I = \frac{|\dot{\gamma}|\, d}{\sqrt{p/\rho}}\,\mathcal{U} = \frac{u_z}{\sqrt{(h - z)}}\,\mathcal{U}. \tag{31}$$

This relation leads to an expression for the z-derivative of u:

$$u_z = \frac{\sqrt{h - z}}{\mathcal{U}}\,\left(\frac{\mu_1 - h_x}{h_x - \mu_2}\right). \tag{32}$$

Then, integration of the relation (32) with the boundary condition $u(z = 0) = 0$ leads to a Bagnold-like profile (see for instance [11]):

$$u = \frac{2}{3\mathcal{U}}\,\left(\frac{\mu_1 - h_x}{h_x - \mu_2}\right)\,[h^{3/2} - (h - z)^{3/2}], \tag{33}$$

We use the continuity equation averaged over the height of the dune (13) for the steady state ($\partial_t = 0$) to evaluate the height of the dune $h(x)$:

$$\frac{\partial}{\partial x}\left(\int_0^h u\,\mathrm{d}z\right) = 0. \tag{34}$$

We integrate this relation with respect to x with the boundary condition $u(x = 0) = \hat{U}_B$ where $\hat{U}_B = U_B/U$ is the dimensionless velocity of the blade with respect to the underlying

layer. Because the table is rotating, this velocity at a given radial position y is $U_B = \Omega\, y$. It leads to

$$\int_0^h u \,\mathrm{d}z = h\, \hat{U}_B. \tag{35}$$

Then with the expression (33) we finally obtain

$$\hat{U}_B = \frac{1}{h} \int_0^h u \,\mathrm{d}z = \frac{2}{5\mathcal{U}} \left(\frac{\mu_1 - h_x}{h_x - \mu_2} \right) h^{3/2}, \tag{36}$$

From this relation, we obtain an equation for the height of the dune at a given distance from the blade $h(x)$ in the limit where the inertial effects are neglected, i.e. at $F \ll 1$:

$$h_x = \frac{\mu_1\, h^{3/2} + F_2\, \mu_2}{h^{3/2} + F_2}, \tag{37}$$

where F_2 is defined by

$$F_2 = \frac{5}{2}\, \hat{U}_B\, \mathcal{U}. \tag{38}$$

Coming back to the dimensional expression, the coefficient F_2 writes:

$$F_2 = \frac{5}{2}\, \frac{U_B\, d}{I_0\, H \sqrt{g\, H}}. \tag{39}$$

We consider the aquarium sand with typical experimental parameters $\Omega = 0.05$ rad/s, $y = y_0 = 25$ cm, $U_B = \Omega\, y$, $H = 5$ cm, $d = 1$ mm, and for I_0, μ_1 and μ_2 the value provided by Jop et al. [9]. The resulting profiles are plotted in figure 8. We can see that the shape of the dune shows some qualitative agreement with the experiments. The profile of the dune is close to a straight slope except when the dune meet the underlying layer where the profile becomes concave as observed in the experiments. However, the analytical theory depends on F_2 which is inversly proportional to $H^{3/2}$. Thus, when the dune becomes smaller, the value of F_2 increases and the profile should change. However, the experiments seem to show the same profile all the time. It may be due that experiments were typically performed with a height of the dune in the range $H \sim 3 - 10$ cm. For smaller height of the dune, the experimental measurements are not sufficiently accurate. Thus, the range of F_2 performed for a given rotation rate does not allow to see a huge variation of F_2. The only way to increase its value is a larger value of the velocity of the blade which will be the point of the next section.

4.4 Influence of the different parameters

The shape observed for aquarium sand, i.e. a straight slope and a curvature near the tip of the dune should be valid for different granular materials in the limit $F \to 0$. Indeed, the analytical model presented in the previous section relies on the $\mu(I)$ rheology which is valid for sand as well as for glass beads. Figure 9(a) illustrates the profile of the dune for 1 mm spherical glass beads and the same parameters as shown in figure 6 after the initial build-up of the dune in the (xz) plane (i.e. approximately after $0.1\, T_{rot}$). Again we can see that the shape of the dune exhibits a curvature near the tip explained by our simple

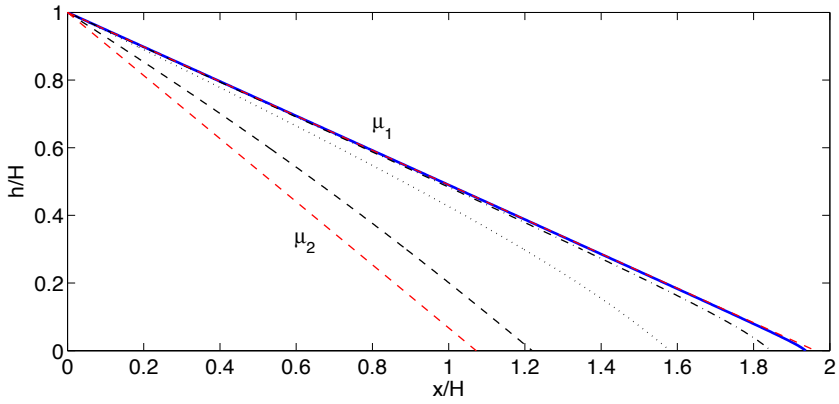

Figure 8: Analytical profile of the dune. The blue continuous line is for the experimental parameters: $H = 6$ cm, $\Omega = 0.05$ rad/s, $y = y_0 = 25$ cm, $U_B = \Omega\, y$, $d = 1$ mm leading to $F_2 = 8.5 \times 10^{-4}$. The red dashed lines indicate the slope given by μ_1 and μ_2.

model. We can also study the influence of the different parameters: the mass (figure 9(b)) or various initial position (figure 9(c)) always in the limit of vanishing Froude number. The profile of the dune seems not to change with these different parameters. Note that with the glass beads the profiles look slightly more curved everywhere. It may be due the shape of the particles which are spherical contrary to the aquarium sand. In this case the p article will be likely incline to roll and the speeds at the surface will increase. This effect is not yet totally understood.

4.5 What about inertia?

We have previously focused on the shape of the dune in the limit where the inertial effects are neglected, i.e. for a Froude number $F \ll 1$. However, experimental observations suggests that the shape of the dune can be modified by inertial effects as illustrated in figure (10) when we increase the rotation rate of the bulldozer. Instead of having an inclined and nearly-flat profile as observed in the previous section, we have a transition to a profile where a significant curvature appears. The profile observed when increasing the Froude number is similar to the "S-shape" observed in rotating drums (see for instance [16]). In figure (10) the Froude number ranges from 0.4 to 1 and its influence has now to be considered to account for the curvature of the profile.

To study the effect of inertia, we consider the leading-order version of (17) with $F = O(1)$. We depth-integrated this equation and use the first order profile (33) obtained previously. It leads to:

$$F^2 \left[\frac{\partial}{\partial t}(hU) + \frac{\partial}{\partial x}\left(\int_0^h u^2 \, \mathrm{d}z \right) \right] = -h_x - \tau_{xz}(x, 0, t) \tag{40}$$

where

$$U = \frac{1}{h} \int_0^h u \, \mathrm{d}z \tag{41}$$

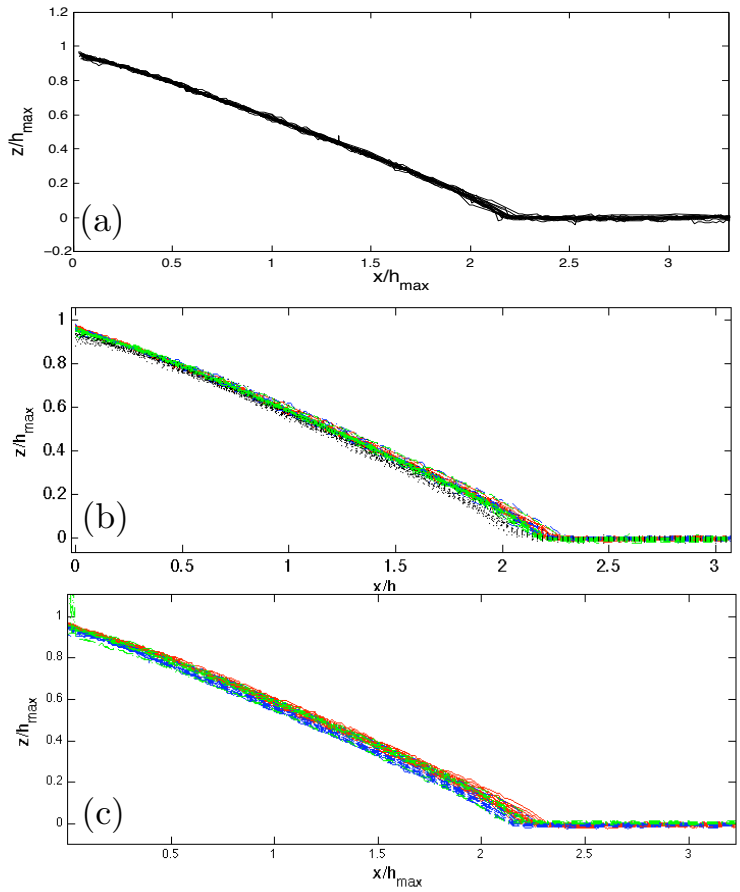

Figure 9: Profile of the dune for the 1 mm spherical glass beads (a) $\Omega = 0.05$ rad/s, $m = 1$ kg, $y = 25$ cm; (b) for the same parameters and various mass: m=1000 g (red), m=750 g (blue), m=500 g (green), m=250 g (black); (c) for various initial radial position: $y_0 = 15$ cm (red), $y_0 = 25$ cm (blue), $y_0 = 35$ cm (green). In all these figures, the time is taken every 10 seconds after the build-up of the dune is achieved.

is the vertical average of the velocity u. To evaluate the inertial terms on the left of this equation and the basal drag, we consider the steady state with constant flux, $(hU)_x = 0$, and exploit the velocity profile of the inertia-less problem, namely

$$u = \frac{5\,U}{3\,h^{3/2}}\,[h^{3/2} - (h-z)^{3/2}] \tag{42}$$

After a little algebra, we arrive at

$$h_x\left(1 + \frac{5\,U^2}{4\,g\,h}\right) = -\mu(I_b). \tag{43}$$

where

$$I_b = \frac{5\,U\,d}{2\,H\,\sqrt{gH}} \tag{44}$$

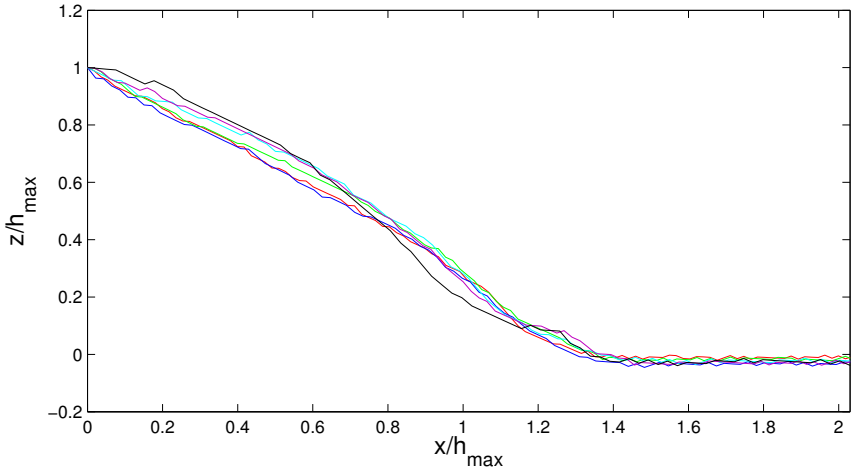

Figure 10: Profile of the dune for different rotation rates $\Omega = 0.8$ rad/s (red), $\Omega = 1$ rad/s (blue), $\Omega = 1.25$ rad/s (green), $\Omega = 1.5$ rad/s (cyan), $\Omega = 1.75$ rad/s (magenta) and $\Omega = 2$ rad/s (black) with $m = 1000$ g, $y_0 = y = 35$ cm and the granular material is the aquarium sand of diameter $d = 0.9$ mm. Profiles are taken at arbitrary times after the build-up of the dune.

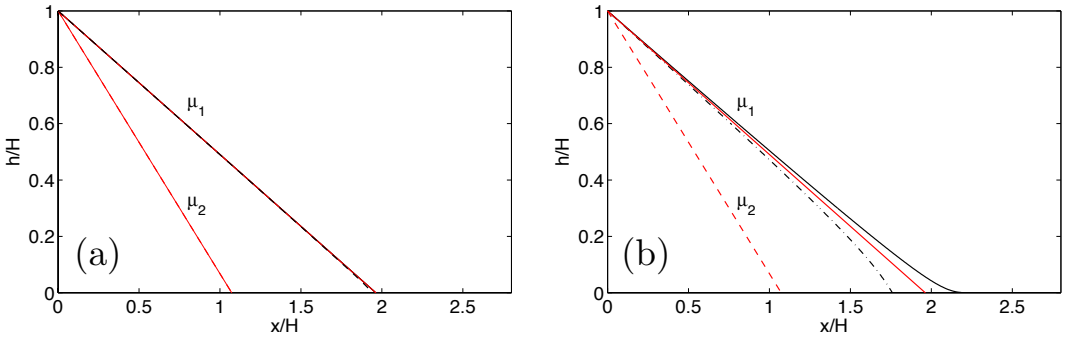

Figure 11: (a) Analytical profile of the dune for the aquarium sand, $y_0 = y = 25$ cm, $d = 1$ mm, $H_0 = 5$ cm and $\Omega = 0.05$ rad/s. (b) Analytical profile of the dune for the aquarium sand, $y_0 = y = 40$ cm, $d = 1$ mm, $H_0 = 5$ cm and $\Omega = 1$ rad/s leading to a larger Froude number. In both figures the black continuous line are obtained with the relation (43) and the black dotted-line are obtained with the relation (37).

Note that this relation is exactly the relation (31) in the limit of vanishing Froude number, i.e. for vanishing velocity U. The term $5\,U^2/(4\,g\,h)$ accounts for the inertial effects. Resulting profiles calculated with this model are shown in figure 11(a) and (b). Figure 11(a) is plotted for a small rotation rate, $\Omega = 0.05$ rad/s. In this case, we see that

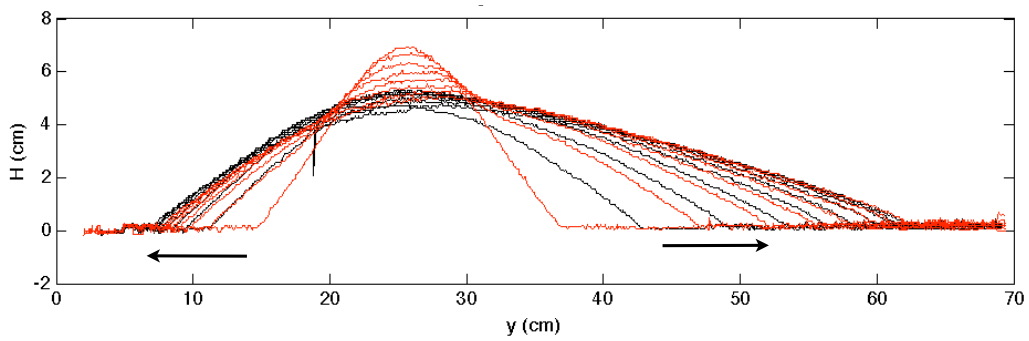

Figure 12: 2D profile of the dune in the plane (yz) for $\Omega = 0.05$ rad/s, $y_0 = 25$ cm, $m = 1000$ g. The granular material used is the 0.9 mm aquarium sand. The red line corresponds to an initial condition where the sand is initially put against the blade whereas the black line indicates the initial condition where a sandpile is set at a distance $y_0 = 25$ cm from the center. The arrows indicate the time-direction.

the profile is similar to the results of the previous section: the Froude number is small. However, for larger velocity, i.e. larger Froude number, the tail of the dune is modified as illustrated by the figure 11(b). The curvature of the profile is more important, as observed experimentally. However, even if the shape of the tail is captured qualitatively, the profile of the dune closer to the blade remains straight in our analytical model whereas in the experiments the curvature is also important in this region.

5 Lateral spreading of the dune

In section 3, we have seen that the motion of the dune can be decomposed into a build-up of the dune perpendicular to the blade and a lateral spreading of the dune along the blade. This lateral spreading effect is present for a rotating blade where the normal velocity to the blade depends on the distance to the center y through the relation $U_\perp = y\,\Omega$. Furthermore, because the front of the blade is position slightly ahead of the centre of the rotating table, there is a tangential velocity along the blade, $U_\parallel$, that advects the dune radially outwards (see below in 5.1.1).

Figure 12 illustrates the two-dimensional dynamics against the blade. Starting from a symmetric sandpile, the dune spreads along the blade and breaks its symmetry: the spreading is faster in this direction where the velocity of the blade is larger.

5.1 Mathematical modelling

5.1.1 Velocity of the bulldozer

First, we calculate the velocity induced by the rotating table at the velocity Ω in the frame of the blade. We use cartesian coordinates where the axis of rotation is at the position $(x = -\delta, y = 0)$ (see figure 13). Introducing r, the distance from the rotating axis, and θ, the angle between the y-axis and $(O_B\,M)$, one can write the coordinates of a point M as

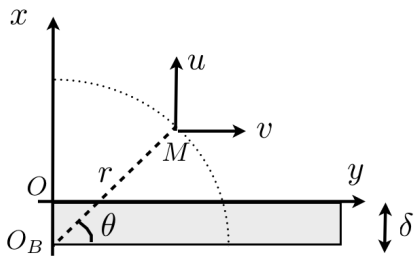

Figure 13: Schematic and coordinates in the (xy) plane. δ is the thickness of the blade. $x = 0$ is taken at the surface of the blade.

$(x_M = r\,\sin\theta - \delta, y_M = r\,\cos\theta)$. Thus the velocity field (U, V) is given by

$$U = -\Omega\, r\,\cos\theta = -\Omega\, y, \tag{45a}$$
$$V = \Omega\, r\,\sin\theta = \Omega\,(x + \delta). \tag{45b}$$

5.1.2 Conservation of mass

Let us express the conservation of mass averaged over z:

$$\frac{\partial h}{\partial t} + \frac{\partial}{\partial x}\left(\int_0^h u\mathrm{d}z\right) + \frac{\partial}{\partial y}\left(\int_0^h v\mathrm{d}z\right) = 0, \tag{46}$$

which can be rewritten as

$$\frac{\partial h}{\partial t} + \frac{\partial}{\partial x}(h\,U + F_x) + \frac{\partial}{\partial y}(h\,V + F_y) = 0, \tag{47}$$

where U (resp. V) accounts for the x-velocity (resp. y-velocity) of the underlying layer in the reference frame of the blade and F_x (resp. F_y) is the flux along the x-direction (resp. y-direction).

5.1.3 Modelling the shape of the dune perpendicularly to the blade

We want to build a simple model of evolution of the shape of the bulldozed dune in the (yz) plane (Fig. 14(a)), thus we need an estimation of the shape of the dune in the direction perpendicular to the blade. From the experimental observations, at low rotation rate, we can assume that for all positions y the slope can be approximated as straight line slope μ which is a parameter of the granular material and height $H(y,t)$ (see Fig. 14(b)). Thus, the equation of the dune in the xz plane can be written as

$$h(x, y, t) = H(y, t) - \mu\, x \tag{48}$$

This is a rough estimation of the shape but largely simplifies the problem from three dimensions to two dimensions.

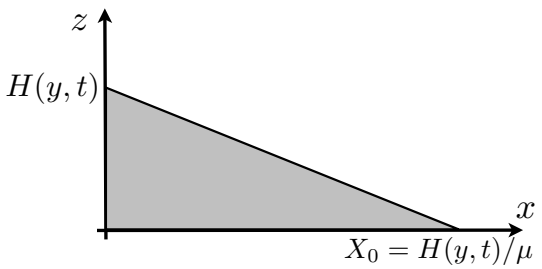

Figure 14: Schematic of the approximated shape of the 2D profile in the plane (xz).

5.1.4 Advection-diffusion equation

Following the experimental observations, our main idea is that adjustments to the granular flow in the x-direction take place relatively quickly, and so the dune is in a quasi-steady state in this direction. This demands that the net horizontal flux in (47), namely $h\,U + F_x$, must be small, with any residual matching the slow time variation of h and weak flux along the blade. That is, $F_x \sim -hU$. To explore the slower lateral spreading and time evolution, we integrate (47) over the x-direction to obtain the relation:

$$\frac{\partial}{\partial t}\left(\int_0^X h\,\mathrm{d}x\right) + \left[h\,U + F_x\right]_0^X + \frac{\partial}{\partial y}\left(\int_0^X h\,V + F_y\,\mathrm{d}x\right) = 0. \tag{49}$$

We evaluate all the terms of this relation with $X = H(y,t)/\mu$. The first term leads to

$$\frac{\partial}{\partial t}\left(\int_0^X h\,\mathrm{d}x\right) = \frac{\partial}{\partial t}\left(\frac{H^2}{2\,\mu}\right) \tag{50}$$

Then, due to the presence of the blade, there is a no-normal flow condition at $x = 0$ which implies that $H(y,t)\,U(x=0) + F_x(x=0) = 0$. At the end of the dune, at $X = H(y,t)/\mu$, by definition the flux drops to zero, i.e. $F_x(x = X) = 0$ and the height of the dune h(x=X) also vanishes. This, the second term of the relation (49) vanishes:

$$\left[h\,U + F_x\right]_0^X = 0. \tag{51}$$

We can separate the last term of the relation (49), and we have:

$$\begin{aligned}\frac{\partial}{\partial y}\left(\int_0^X h\,V\,\mathrm{d}x\right) &= \frac{\partial}{\partial y}\left(\int_0^X h\,\Omega\,(x+\delta)\mathrm{d}x\right),\\ &= \frac{\partial}{\partial y}\left(\frac{\Omega\,\delta\,H^2}{2\,\mu^2} + \frac{\Omega\,H^3}{6\,\mu^2}\right).\end{aligned}$$

For a free-surface gravity-driven flow, one expects that the flux, $\mathbf{F} = (F_x, F_y)$, is proportional to the surface slope. That is, $\mathbf{F} \approx -\Gamma\nabla h$, where the factor Γ encapsulates the detailed physics of the granular flow. For example, for the shallow, inertia-less flow described by the $\mu(I)$ law in section 4, one can generalize the analysis and find

$$\Gamma = \frac{2\,I_0\,\sqrt{g}}{5\,d}\,\frac{h^{5/2}}{|\nabla h|}\left(\frac{\mu_2 - \sqrt{{h_x}^2 + {h_y}^2}}{\sqrt{{h_x}^2 + {h_y}^2} - \mu_1}\right) \tag{52}$$

Hence,

$$F_y \approx F_x \, \frac{h_y}{h_x} \approx -\frac{h\,U\,H_y}{\mu} \tag{53}$$

given our assumptions on the quasi-steady profile in x ($F_x \approx -h\,U$ and (48)). After integration we obtain

$$\frac{\partial}{\partial y}\left(\int_0^X F_y \,\mathrm{d}x\right) = \frac{\partial}{\partial y}\left(\frac{H^2\,H_y}{2\,\mu^2}\Omega\,y\right). \tag{54}$$

In conclusion, the relation (49) leads finally to the evolution equation for $H(y,t)$:

$$\frac{\partial H^2}{\partial t} + \frac{\partial}{\partial y}\left(\Omega\,\delta\,H^2 + \frac{\Omega\,H^3}{3\,\mu}\right) + \frac{\partial}{\partial y}\left(\frac{H^2\,H_y}{\mu}\Omega\,y\right) = 0. \tag{55}$$

Note that this equation is an advection-diffusion equation which can be solved using a defined initial condition. The initial height will be choosen to fit with the initial sandpile.

5.2 Time-evolution of the dune

We can solve the partial differential equation (55) numerically. An example of the profile obtained is plotted in figure (15.a). This profile is plotted for the parameter used in the experimental results shown in figure (15.b). First, the thickness of the blade, $\delta = 1$ cm, is directly measure on the experimental setup. The slope of the dune perpendicularly to the blade is obtained from experiments done in section 4: $\mu \simeq \tan(40\,\pi/180)$ for the aquarium sand. In addition, note that the diffusivity in (55) vanishes in the limit $H \to 0$. To avoid the implied singularity, the computation also includes a pre-wetted layer everywhere, i.e. the initial condition are:

$$H(y, t=0) = \max(H_0 - \mu\,|y - y_0|) + \gamma_0, \tag{56}$$

where γ_0 is the thickness of the pre-wetted layer and $\max(H_0 - \mu\,|y - y_0|)$ is a triangular function centered in y_0 of height H_0. H_0 is chosen as an adjustement parameter.

We can see that the spreading of the dune is non-symmetric and the maximum height of the dune travels outward with time. Although the agreement is not quantitative, the qualitative feature of the lateral spreading is well captured by our simple toy-model. In addition this maximum height decreases during the spreading in a qualitative good agreement.

6 Conclusion

In this project, we have studied the dynamics of bulldozed sand using experimental characterizations and some qualitative modelling with granular rheology. The experiments were performed with a rotating bulldozer which allows us to demonstrate that the dynamics of the dune built against the blade can be split into two phases. A first adjustment takes place transverse to the blade, with the dune adopting a quasi-steady profile with almost constant slope. The profile can be qualitatively reproduced with a shallow 2D flow model incorporating the so-called $\mu(I)$-rheology. The transverse adjustment is followed by a second phase of lateral spreading. A crude model of this second phase reproduces the asymmetrical spreading of the dune along the blade and its gradual outward migration.

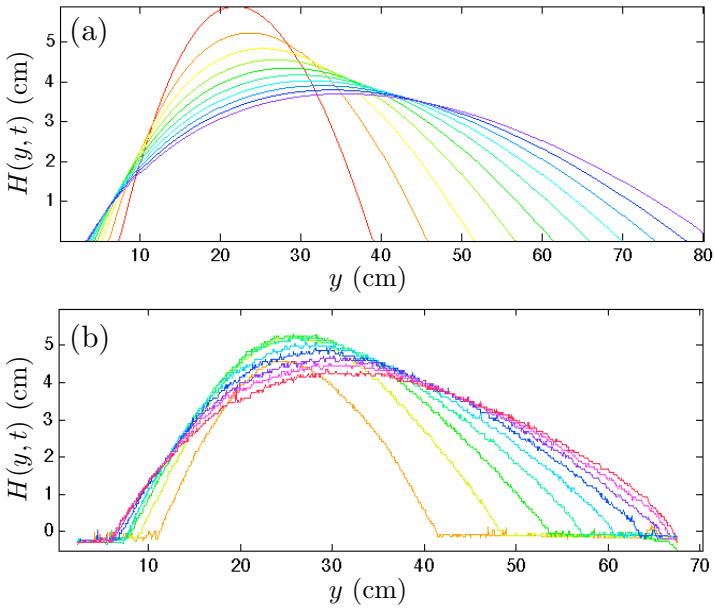

Figure 15: (a) Analytical profile with $\Omega = 0.05$ rad/s, $y_0 = 20$ cm, $\mu = \tan(40\,\pi/180)$, $\delta = 1$ cm, $H_0 = 9$ cm, $\gamma_0 = 0.01$ cm. (b) Experimental profile obtained with the aquarium sand for $\Omega = 0.05$ rad/s, $y = y_0 = 20$ cm. The profiles are taken every 5 seconds.

We have outlined in this report results based on experiments and suggested analytical modeling of the observed flow. However, one can notice that it exists some discrepancies between the theory and experiments. It may be due to some strong assumptions: the flow perpendicular to the blade was assumed to be shallow which is not totally satisfied. In addition, we used a quasi-steady assumption to split the dynamics into two phases and study them separately, but there may be some interplay between the 2D dynamic and the lateral spreading.

To further understand the dynamic of bulldozed material, extensions of the theory can be done by considering a fully 2D modeling of fluid with a $\mu(I)$-rheology, i.e. without shallow-water approximations. We will carry 2D particle dyamics with a DEM code to study the flow without lateral spreading. Numerical simulations allow us to have access to various physical quantities such as the velocity inside the dune or the transient shape during the build-up of the dune. Numerical simulation with a $\mu(I)$ rheology [11] can also be compared to DEM simulation to study if the dynamic of the dune can be indeed captured by the $\mu(I)$ rheology.

We will also extend the experiments by performing PIV measurement to obtain the velocity field at the surface of the dune. Some experiments to see if there is any particle exchange between the dune and underlying bed are also needed. We outlined that the sandpaper allow no-slip boundary condition, but examining effects of slip by removing sandpaper would also be interesting as well as studying slower speeds and other materials to look for unsteady avalanching.

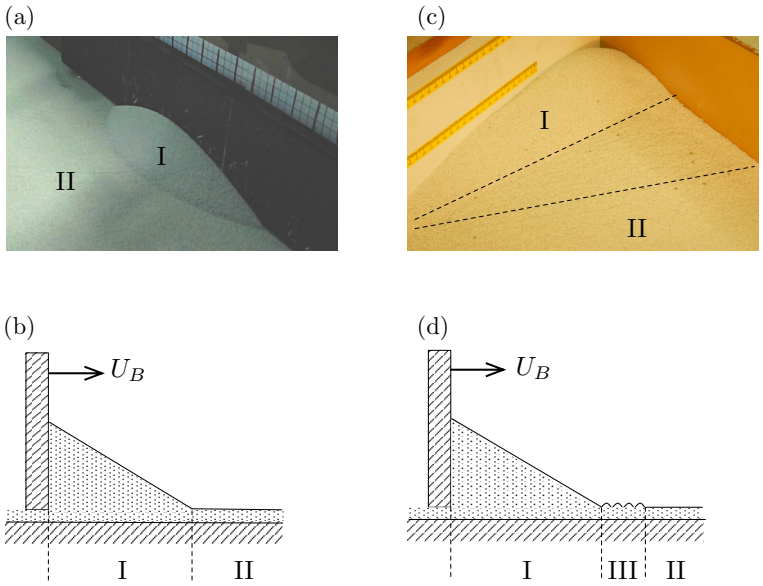

Figure 16: Photo and schematic of bulldozed sand by a blade at velocity U_B for no-slip (a,b) and slip (c,d) boundary conditions at the bottom. I, II and III denotes the three distinct regions which are visible: (I) a dune, (II) a horizontal layer of sand far from the blade, (III) a region where the granular materials is squeezed in a wrinkled layer before being bulldozed.

A Slipping or not slipping?

Depending on the coating of the rotating table, two different regimes can be observed for the bulldozed sand (see figure 16). If the table is coated with sandpaper, the boundary condition at the bottom are no-slip boundary condition. In this case, we observed two different zones: a zone where the sand is bulldozed and a zone far from the blade where the granular material is stationary (see figure 16a.b). This is this situation we study in this report.

However, in the absence of sandpaper on the bottom, the boundary condition on the table is less obvious. There is likely a sliding layer of grain. In this case, the avalanching dune is buffered from the upstream static bed by a compressing, sliding layer of grains. In some exploratory experiments, this layer appeared to lose stability towards a type of buckling instability, rendering the free surface into a wavy pattern (region III on figure 16c.d). This situation is more complicated to describe as the characteristic of the surface becomes really important. This new situation would deserved a proper study in the future but is beyond the scope of this report.

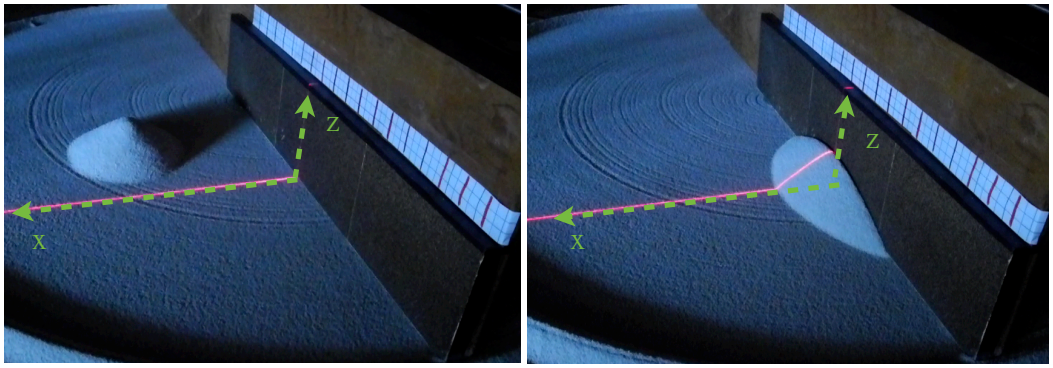

(a) (b)

Figure 17: Laser sheet projected on the table (red line). (a) For a flat topography the line remains straight, the height is equal to $h = 0$. (b) When the dune is present, the deviation of the line from a straight line leads to the value of $h(x)$ after initial calibration.

B Diagnostic method: calibration and topography of the dune

In addition to the qualitative visualization of the bulldozing phenomenon, we need to have access to quantitative features. Here, we want to obtain the shape of the dune at an arbitrary radius. However, we need a non intrusive method. We have used a method developed during the summer which relies on the deformation of a laser line projected on a topography. For this method, we project a sheet at a given radius. In the absence of topography, a straight line is observed (see figure 17(a)). However, as soon as a topography is present, the sheet is deformed (see figure 17(b)) and we can measure the distance between the deformed and non-deformed line to have access to the height.

Note that the movie has to be recorded by a camera located in a position such that we can see the whole topography of the dune. Figures 17(a) & 17(b) show a typical example of view to study the entire topography of the dune. However, as can be seen on these two figures, it leads to some problems to describe the topography of the dune as a function of the variables (x, y, z). Indeed the view is $3D$, thus the axis (Ox) and (Oz) are not perpendicular, in addition the length scales change with the position. Therefore, before postprocessing the movies, we need to calibrate the position of the camera to obtain a direct correspondence between the location of a pixel (x_p, z_p) and the physical values (x, y, z).

We use a squared board at a given radial position y. One calibration will be valid only for a given value of y which will be the position of our laser sheet (note that in figure 18, y is known from the scale on the top of the blade). Then, we obtain the direction of the axis (Ox) and (Oz) from the edges of the board. Because the axis are not perpendicular, we need to determine the vanishing points which allow us to correct the effects of the perspective. It corresponds to the intersection of the red dashed line in figure 18). Then, we determine the length scales along y and z with the graduation on the grid. In a first approximation, direct measurements show that the correspondence between the measured distance on the

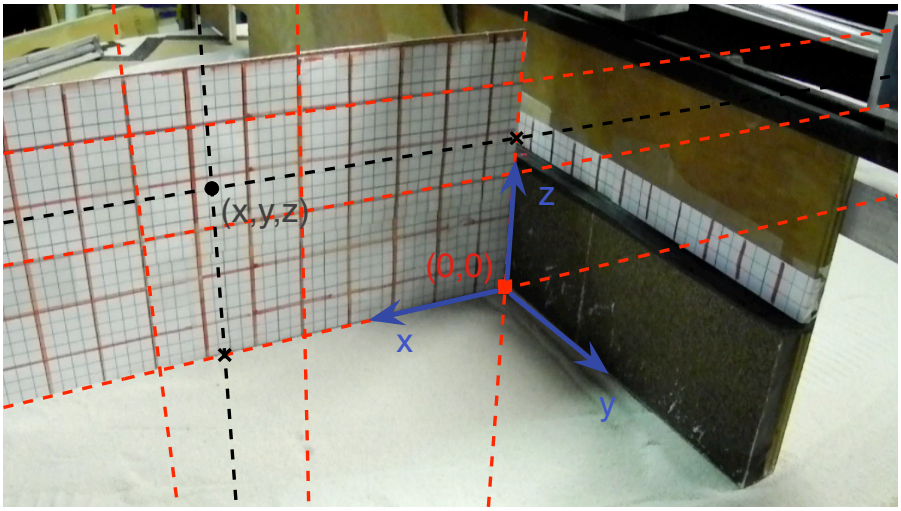

Figure 18: Photo of the calibration process. The board is used to define the direction of the axis, the vanishing points and the lengthscales.

picture and the real distance is linear. After this calibration, we consider a pixel at a known location (x_p, z_p) in our movie, then we project this point on the (Ox) and (Oz). Using the length scales determine during the calibration process, we obtain the location (x, z) for a given y.

Acknowledgments: Developing an experimental setup from scratch in few weeks has been a difficult but fantastic experience. It would have definitely not be possible without the numerous ideas, the reactivity and the enthusiasm throughout the summer of Neil Balmforth and Colm Caulfield. Thank you for introducing me to the topic of granular material, both experimental and theoretical. We started from a basic idea, what happen if we bulldoze some sand. Then, we encountered some problems during the realization which have been solved one by one and finally our rotating bulldozer was working! These experiments with granular material would not have been possible without Claudia Cenedese's tolerance of so much dust in the lab! I am also grateful to Anders Jensen for many technical innovations on our setup. To conclude, I also would like to thank all the staff and fellows of the GFD Summer Program. Spending the summer at Walsh Cottage provided me an unique educational opportunity and incredible experience.

References

[1] B. Andreotti, *Sonic sands*, Rep. Prog. Phys., 75 (2012), p. 026602.

[2] R. Bagnold, *The shearing and dilatation of dry sand and the singing mechanism*, Proc. Roy. Soc. A, 295 (1966), pp. 219–232.

[3] A.-F. Bitbol, N. Taberlet, S. Morris, and J. McElwaine, *Scaling and dynamics of washboard roads.*, Phys. Rev. E, 79 (2009), p. 061308.

[4] F. Da Cruz, *Écoulements de grains secs: forttement et blocage*, thèse de l'école nationale des ponts et chaussèes, Université de Nice Sophia-Antipolis, 2004.

[5] S. Douady, A. Manning, P. Hersen, H. Elbelrhiti, S. Protiere, A. Daerr, and B. Kabbachi, *The song of the dunes as a self-synchronized instrument*, Phys. Rev. Lett., 97 (2006), p. 018002.

[6] Y. Forterre and O. Pouliquen, *Flows of dense granular media.*, Annu. Rev. Fluid Mech., 40 (2008), pp. 1–24.

[7] K. Hutter, T. Koch, C. Pluss, and S. Savage, *The dynamics of avalanches from initiation to runout. part ii: experiments.*, Acta Mechanica, 109 (1995), pp. 127–165.

[8] P. Jop, Y. Forterre, and O. Pouliquen, *Crucial role of side walls for granular surface flows: consequences for the rheology.*, J. Fluid Mech., 541 (2005), pp. 167–192.

[9] ——, *A constitutive law for dense granular flows.*, Nature, 441 (2006), p. 727.

[10] L. Lacaze and R. Kerswell, *Axisymmetric granular collapse: a transient three dimensional flow test of viscoplasticity.*, Phys. Rev. Lett., 102 (2009), p. 108305.

[11] P.-Y. Lagrée, L. Staron, and S. Popinet, *The granular column collapse as a continuum: validity of a two-dimensional navier-stokes model with a $\mu(i)$-rheology.*, J. Fluid Mech., 686 (2011), pp. 378–408.

[12] G. Midi, *On dense granular flows.*, Eur. Phys. J. E., 14 (2004), pp. 341–365.

[13] B. Percier, S. Manneville, J. McElwaine, S. Morris, and N. Taberlet, *Lift and drag forces on an inclined plow moving over a granular surface*, Phys. Rev. E, 84 (2011), p. 051302.

[14] S. Savage and K. Hutter, *The dynamics of avalanches of granular materials from initiation to runout. part i: analysis.*, Acta Mechanica, 86 (1991), pp. 201–223.

[15] N. Taberlet, S. Morris, and J. McElwaine, *Washboard road: The dynamics of granular ripples formed by rolling wheels*, Phys. Rev. Lett., 99 (2007), p. 068003.